SMC-TR-95-37

AEROSPACE REPORT NO.
TR-94(4935)-13

Photochemically Deposited Contaminant Film Effects: Data Archive

Volume 1

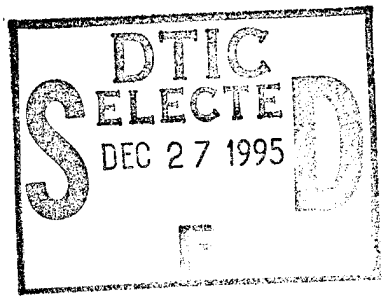

15 September 1994

Prepared by

G. S. ARNOLD and K. LUEY
Mechanics and Materials Technology Center
Technology Operations

Prepared for

SPACE AND MISSILE SYSTEMS CENTER
AIR FORCE MATERIEL COMMAND
2430 E. El Segundo Boulevard
Los Angeles Air Force Base, CA 90245

Engineering and Technology Group

THE AEROSPACE CORPORATION
El Segundo, California

This report was submitted by The Aerospace Corporation, El Segundo, CA 90245-4691, under Contract No. F04701-93-C-0094 with the Space and Missile Systems Center, 2430 E. El Segundo Blvd., Los Angeles Air Force Base, CA 90245. It was reviewed and approved for The Aerospace Corporation by S. Feuerstein, Principal Director, Mechanics and Materials Technology Center.

This report has been reviewed by the Public Affairs Office (PAS) and is releasable to the National Technical Information Service (NTIS). At NTIS, it will be available to the general public, including foreign nationals.

This technical report has been reviewed and is approved for publication. Publication of this report does not constitute Air Force approval of the report's findings or conclusions. It is published only for the exchange and stimulation of ideas.

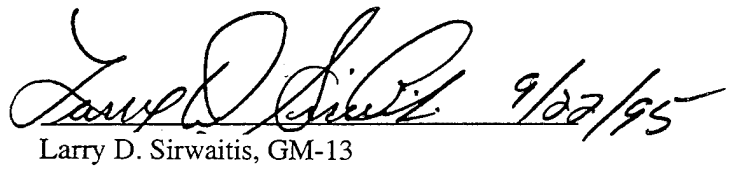

Larry D. Sirwaitis, GM-13
Ch, Program Protection Branch
Directorate, Acquisition Security

REPORT DOCUMENTATION PAGE

Form Approved
OMB No. 0704-0188

1. AGENCY USE ONLY (*Leave blank*)	2. REPORT DATE	3. REPORT TYPE AND DATES COVERED
	15 September 1994	

4. TITLE AND SUBTITLE

Photochemically Deposited Contaminant Film Effects: Data Archive

5. FUNDING NUMBERS

F04701-93-C-0094

6. AUTHOR(S)

G. S. Arnold and K. Luey

7. PERFORMING ORGANIZATION NAME(S) AND ADDRESS(ES)

The Aerospace Corporation
Technology Operations
El Segundo, CA 90245-4691

8. PERFORMING ORGANIZATION REPORT NUMBER

TR-94(4935)-13

9. SPONSORING/MONITORING AGENCY NAME(S) AND ADDRESS(ES)

Space and Missile Systems Center
Air Force Materiel Command
2430 E. El Segundo Boulevard
Los Angeles Air Force Base, CA 90245

10. SPONSORING/MONITORING AGENCY REPORT NUMBER

SMC-TR-95-37

11. SUPPLEMENTARY NOTES

12a. DISTRIBUTION/AVAILABILITY STATEMENT

Approved for public release; distribution unlimited

12b. DISTRIBUTION CODE

13. ABSTRACT (*Maximum 200 words*)

Perhaps the most pernicious types of spacecraft contaminants are photochemically deposited ("solarized") molecular films. This report documents the results from a project aimed at improving control of thermo-optical effects of contamination in the design of spacecraft. Photodeposition results and analyses of the ultraviolet and visible transmission spectra of films from several organic precursor molecules are reported. The major differences among contaminant film types have been found to be in the initial photodeposition propensity, rather than in the ultimate optical properties of the films.

14. SUBJECT TERMS

Contamination, Photochemical deposition, Quartz crystal microbalance, solar absorptance

15. NUMBER OF PAGES

327

16. PRICE CODE

17. SECURITY CLASSIFICATION OF REPORT	18. SECURITY CLASSIFICATION OF THIS PAGE	19. SECURITY CLASSIFICATION OF ABSTRACT	20. LIMITATION OF ABSTRACT
UNCLASSIFIED	UNCLASSIFIED	UNCLASSIFIED	

Preface

This work was supported by the U.S. Air Force Space and Missile Systems Center under contract number F04701-88-C-0089.

The contributions of Mr. David F. Hall and Dr. H.K. Alan Kan in the genesis of this work are gratefully acknowledged. The initial definition of the matrix of materials to test rests upon the work of Mr. Henry S. Judeikis. Mr. Michael Yao wrote the laboratory data acquisition software, which has served this effort well. Ms Rolaine C. Young Owl participated in much of the data acquisition.

The reduction and analysis of data was performed using the Aerospace Technology Operations Digital Information Research and Analysis Center (DIRAC). DIRAC is a portion of the scientific and technical legacy of the late Dr. Charles M. Randall and it is ably managed by Ms Lynn Friessen and Ms Fong Tien, to the great benefit of The Aerospace Corporation. The preparation of this report relied upon the Technology Operations "ASTRA" computer network, which is supported and maintained by Mr. Herb Hedgepeth.

This reported is published in two volumes. This first volume contains the main text of the report. A second volume contains the four appendices which document the measured contaminant optical transmission spectra and their fitting to describe the contaminants' effects. Most of the recipients of the initial distribution of this report will receive only the first volume. The second is available, on request, from the The Aerospace Corporation's Charles Lauritsen Library.

Contents

Figures

Tables

1. Introduction

1.1 Background

Spacecraft function in a hostile environment of sunlight, charged particles, debris and micrometeoroids, the residual atmosphere, and self-contamination. This environment adversely affects thermal and optical properties of spacecraft surfaces. Operational experience on GPS, DMSP, DSP, and CDP spacecraft and on dedicated experiments has shown that *radiators, solar power arrays, and optical elements in sensors* are degraded in performance by contamination.[1,2,3] As mission durations increase, along with pressures for greater economy in design and operation, the importance of accurately assessing long-term environmental effects and for devising cost-effective strategies to mitigate those effects increases.

Perhaps the most pernicious types of contaminants are photochemically deposited ("solarized") molecular films.[4] The magnitudes of the effects of these films on thermal control and solar photovoltaic surfaces are difficult to predict with high reliability. This uncertainty has two primary origins. Spacecraft contaminant films are not made of pure, well characterized materials, and, once they are deposited, they can be further "darkened" by energetic radiation in the natural space environment.

This report documents the results from a project aimed at improving control of thermo-optical effects of contamination in the design of spacecraft. The goal of this work is to provide the basic data needed to guide materials selection based on the effects of the contaminant films they produce, as well as the quantity of material they outgas.[5]

1.2 Approach

The philosophy, design, and initial results of this work have been reported previously.[6,7] The approach taken is threefold:

1. A spacecraft nonmetallic materials list was analyzed to predict the sorts of compounds that will outgas from these materials, becoming contaminant film precursors.

2. The effects of the geosynchronous space environment on the various classes of outgassers were estimated.

3. Experimental measurements were made of the optical properties of contaminant films photochemically deposited from a list of model precursors, under simulated space environment conditions.

The first two subjects were addressed in Reference 6. This report archives additional experimental results, including optical spectra of four types of photodeposited films.

An important element of our approach is the use of pure substances as model contaminants to represent the outgassing products of spacecraft materials. This approach has been used successfully in this and other laboratories to reveal details of the kinetics and thermodynamics of spacecraft surface contamination.[4,8] It is also practical in that it allows better control over the rate of film deposition and its composition over the course of measurements that last up to 30 days. This report will not specifically address the validity of the model compound selections; that is a subject of continuing research that will be reported later.

1.3 Report Structure

This report is an archive of the data acquired and reduced to date in this project. Analysis of the *reduced* data captured here, addressing the absolute effects of the contaminant films on thermal control and solar photovoltaic surfaces and their comparison to the existing flight test and ground simulation data base, will be presented in future reports.

Section 2 of this report briefly recapitulates the contaminant model material selection, describes the apparatus, and reports the deposition results. Section 3 shows the measured transmission spectra of the photodeposited films and describes the reduction of these spectra to apparent absorption coefficients. Section 4 provides some discussion and indication of planned future work to analyze these results.

The detailed fit results for the four materials studied are presented graphically and in tabular form in separate appendices.*

* Each appendix is approximately 70 pages in length. Since they were prepared to provide stand-alone archives of the reduced data for each material, there is a degree of redundancy among the appendices and between the appendices and the main report. Most copies of this report are distributed without the appendices. They are available from the author on request.

2. Photochemical Deposition

2.1 Model Contaminants

The selection of model contaminants is described in reference 6. The process can be described briefly as follows. A list of materials, their total masses, and outgassing characteristics as described by ASTM E-595 was obtained for a typical spacecraft from a major United States spacecraft prime contractor. Based on the chemical composition of the materials (and when available, the composition of outgassing species), thermal aging data, and radiation-induced offgassing data, a collection of generic classes of molecules representative of space hardware outgassing was developed. For each class of molecules, one or more representative pure substances were selected and procured. Table 1 lists the classes of outgassing materials, their sources, and the analog or "model" contaminant(s) selected.

One additional criterion used to select the model contaminants was their (known or estimated) vapor pressure. This was to facilitate handling and provide for readily controllable deposition conditions.

Table 1. Contaminant Analog Molecules

Material	Sources	Abundance*	Model Contaminant (aliases)
Phthalates	Polyesters, Urethanes	High	di(2-ethylhexyl)phthalate (dioctyl phthalte, DEHP)
Phenols	Epoxies	High	4-4'-isopropylidene phenol (bisphenol-a, bisphenol)
Polybenzimidizoles	Kapton®	High	n-phenylphthalimide
Aromatic Hydrocarbons	Multiple	High	bibenzyl dodecahytrotriphenylene (DTP)
Aromatic Amines	Urethanes, Epoxies	Low	4-tetradecylanaline
Silicones	Silicones (RTV's)	Medium	tetramethyltetraphenyl trisiloxane (DC704)
Alkenes	Multiple	Medium	squalene
Aliphatic Carbonyls	Multiple	Medium	10-nonadecanone

* Abundance estimates are based on the material survey described in Reference 6.

2.2 Apparatus

Figure 1 shows a photograph of the contamination deposition and effects facility. Its major elements are shown schematically in Figures 2 and 3. It is described in detail in Reference 6. There are three functional levels of the experiment. The middle plane is the deposition plane, at which the target is exposed to an organic effluent and VUV photons. The upper plane is for irradiation of a previously deposited film by electrons, ions, and photons. At the lower plane, the transmission spectrum of the film, deposited on Corning 7940 high purity fused silica, is measured using a Cary spectrophotometer.

The entire experiment, deposition, irradiation, and measurement, is carried out inside an ultra-high vacuum chamber equipped with crushed metal seals and evacuated with a turbomolecular pump and a liquid nitrogen cooled shroud. The film thickness is monitored using a custom-built, 10 Mhz, doublet, temperature controlled, quartz crystal microbalance (QCM or TQCM).

The depositions described in this report were performed using two VUV lamps. The lamps' intensities were not continuously monitored. Measurements performed earlier indicate that the illumination provided corresponded roughly to 1 VUV sun intensity for the 130-190 nm range.[4] Care was taken in the selection of the source and deposition surface temperatures to ensure that **no steady-state film deposition occurred in the absence of either the contaminant flow or the VUV irradiation.**

Transmission spectra of the films deposited on a Corning 7940 fused silica* substrate were measured, *in situ*, using a Cary 14 spectrophotometer equipped with an after market data acquisition and baseline correction system (LUSI II**). Visible wavelength range data were acquired from 700-350 nm; ultraviolet data were measured from 395-225 nm. The spectrometer was operated in a fixed slit width mode to ensure that, within any particular spectrum, the area of the film sampled remained constant.

TQCM data, temperature measurements, and optical spectra were recorded using an IBM AT® computer using ASYST® laboratory data acquisition software. Data reduction was performed using the Aerospace Technology Operations Digital Information Research and Analysis Center's DEC VAX computers and Interactive Data Language®.

---

* Obtained from Optical Coating Laboratory, Inc.

** Spectra Instruments

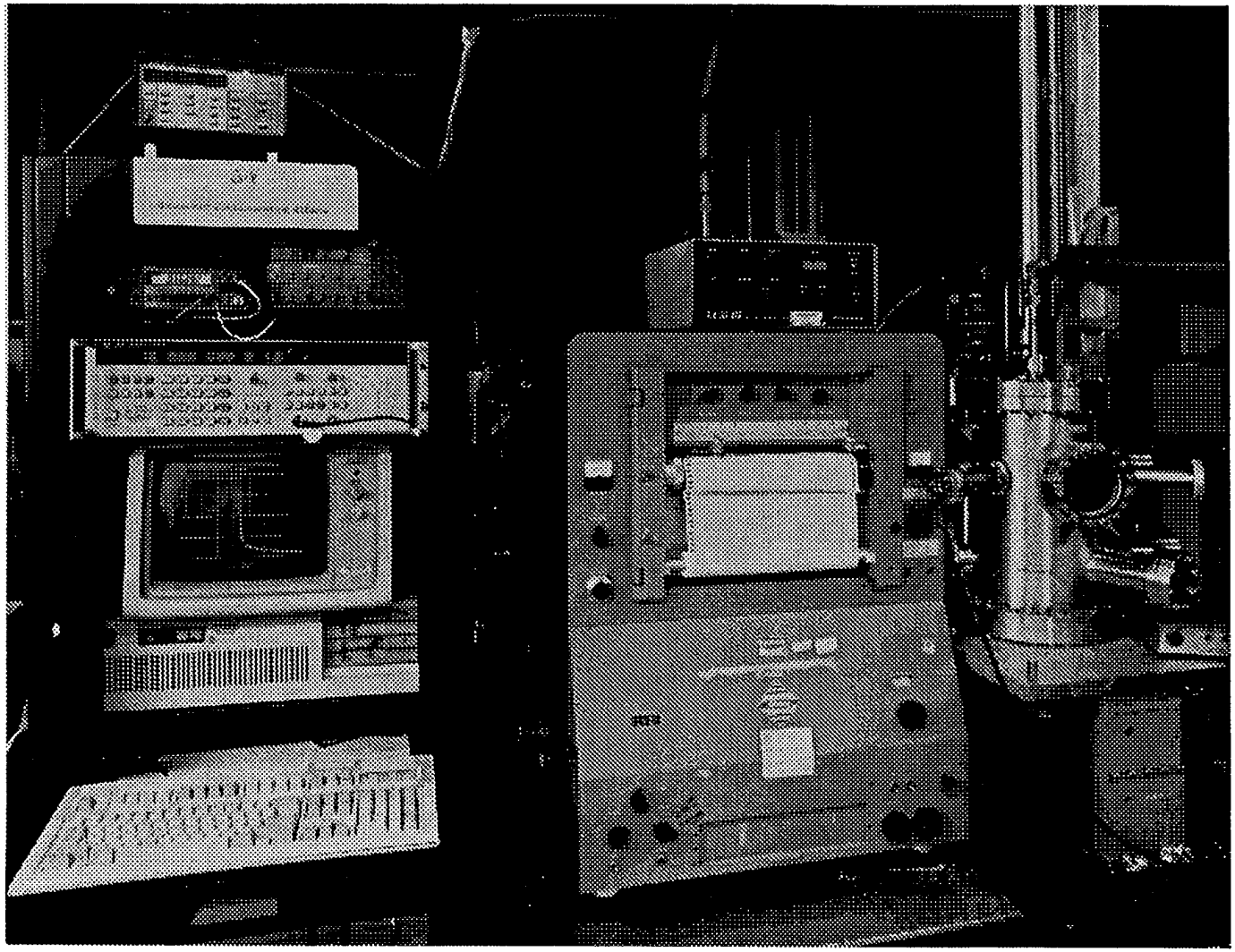

Figure 1. Photograph of the contamination deposition and effects facility ($\Delta\alpha$).

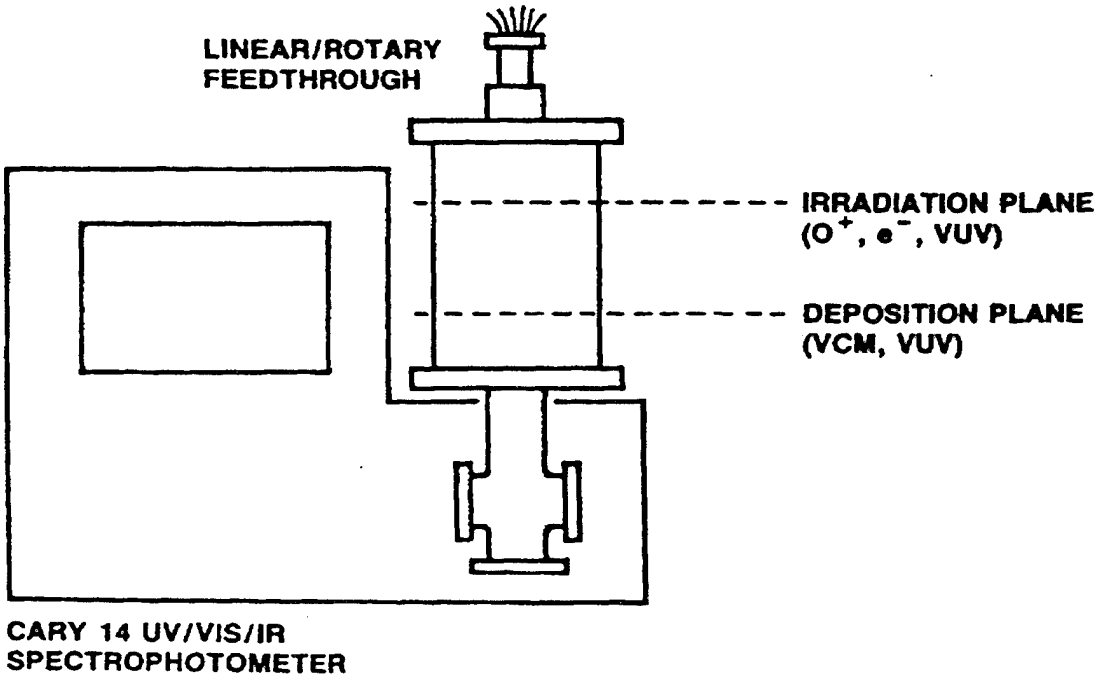

Figure 2. Schematic representation of the contaminant deposition and effects facility, elevation view.

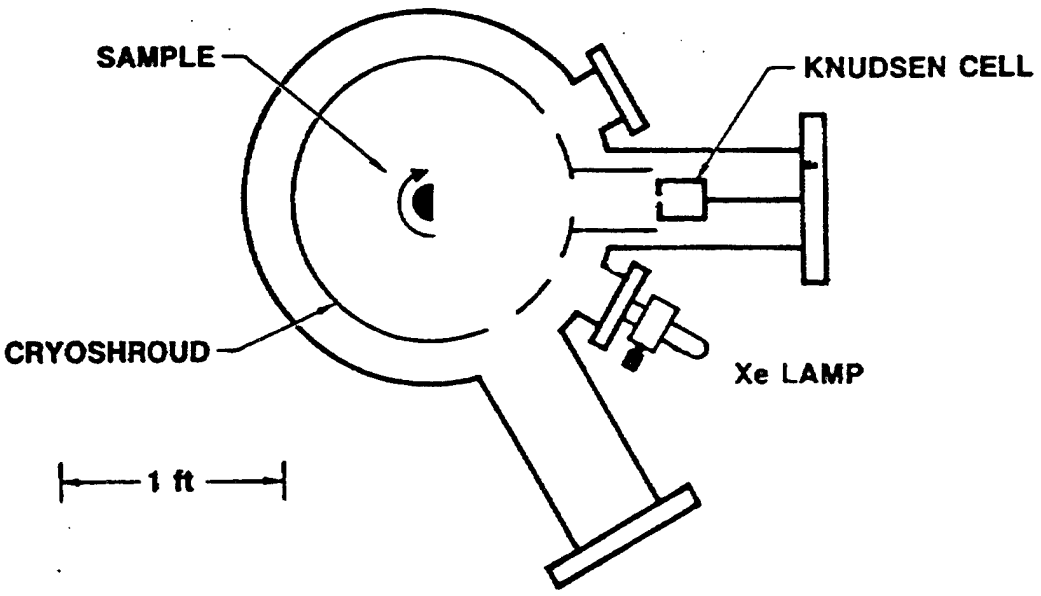

Figure 3. Schematic representation of the contaminant deposition and effects facility deposition plane, plan view. Note that during these tests, two Xe VUV resonance lamps were used.

2.3 Results

Deposition measurements have been performed for seven contaminant analogs, representative of six of the eight classes of materials described in Table 1. Table 2 summarizes the results of those measurements. Note that attempts to photodeposit the aromatic hydrocarbons and the aliphatic carbonyl using 150-180 nm radiation were unsuccessful, even though it was possible to maintain surface concentrations of the materials similar to those used in the successful depositions.[7]

Figures 4-7 show the TQCM data measured during the photochemical deposition of the four materials. The films grew at a rates between 1-2 Hz/hour (0.04-0.09 nm/hour) throughout most of the multiple day experiments. The occasional spikes in the TQCM temperature, and the corresponding spikes in the beat frequency, occur when the test fixture is moved out of the field of view of the cryoshroud to measure the transmission spectrum.

Table 2. Deposition Results Summary

Material	Sources	Model Contaminant (aliases)	Depositon Rate (nm/hr)
Phthalates	Polyesters, Urethanes	di(2-ethylhexyl)phthalate (dioctyl phthalate, DEHP)	0.06
Phenols	Epoxies	4-4'-isopropylidene phenol (bisphenol-a, bisphenol)	0.04
Polybenzimidizoles	Kapton®	n-phenylphthalimide	
Aromatic Hydrocarbons	Multiple	bibenzyl	No Photodeposition
		dodecahytrotriphenylene (dtp)	No Photodeposition
Aromatic Amines	Urethanes, Epoxies	4-tetradecylanaline	*
Silicones	Silicones (RTV's)	tetramethyltetraphenyl-trisiloxane (DC704)	0.08
Alkenes	Multiple	squalene	0.04
Aliphatic Carbonyls	Multiple	10-nonadecanone	No Photodeposition

* The tetradecylanaline measurement is in progress at the time of this writing. The material exhibits a deposition rate similar to the phenol.

In very slow depositions, such as these, fluctuations in the source temperature, the shroud temperature, and the QCM and QCM heat sink temperature can cause variations in the deposition rate. However, for the most part, the films increased in thickness (density) continuously, at nearly constant rates.

Note that toward the end of the squalene deposition, the QCM beat frequency output became very noisy. This anomalous noise is most probably related to grounding problems in the QCM test fixture. However, because of the high sampling frequency (1 QCM measurement every 20 seconds), one can readily distinguish the rapid, anomalous shifts from the actual trend in the data. Therefore, it was possible to discern the apparent film thicknesses to the required precision.

The nominal film thicknesses were calculated assuming a density equal to that of the starting material and a TQCM calibration coefficient of 4.43 ng/cm^2/Hz.[9]

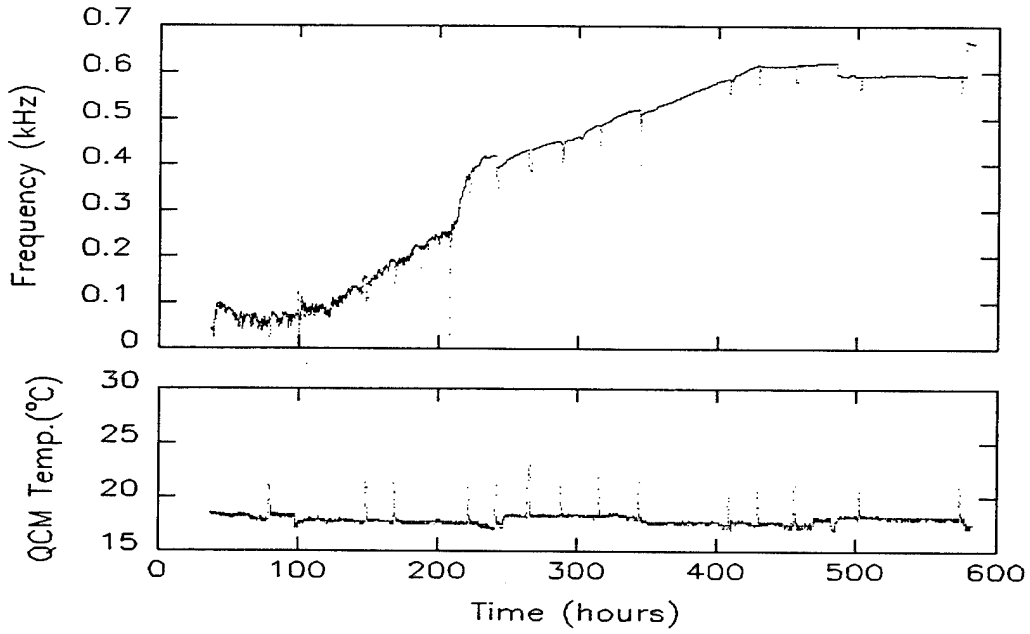

Figure 4. Temperature controlled quartz crystal microbalance measurements taken during the photochemical deposition of bisphenol. The top panel shows the TQCM beat frequency. The bottom panel shows the TQCM temperature.

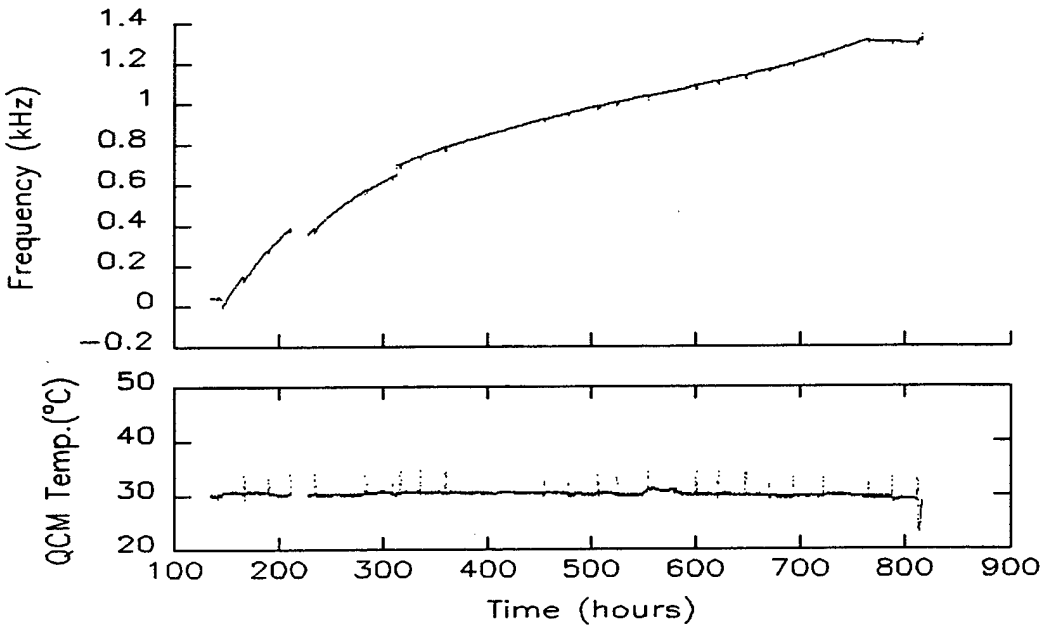

Figure 5. Temperature controlled quartz crystal microbalance measurements taken during the photochemical deposition of DC704. The top panel shows the TQCM beat frequency. The bottom panel shows the TQCM temperature.

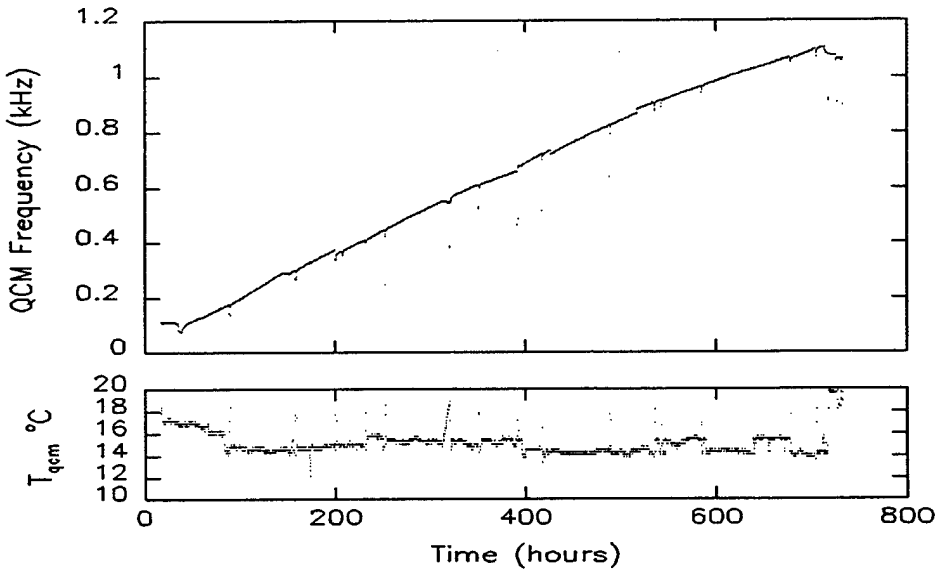

Figure 6. Temperature controlled quartz crystal microbalance measurements taken during the photochemical deposition of DEHP. The top panel shows the TQCM beat frequency. The bottom panel shows the TQCM temperature.

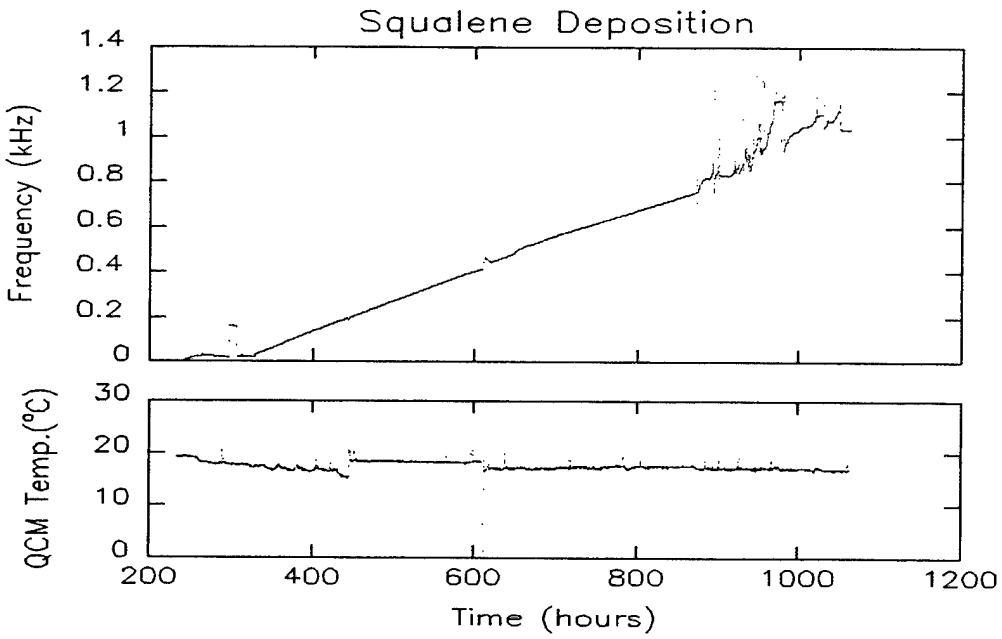

Figure 7. Temperature controlled quartz crystal microbalance measurements taken during the photochemical deposition of squalene. The top panel shows the TQCM beat frequency. The bottom panel shows the TQCM temperature.

3. Spectra of Photochemically Deposited Films

3.1 Typical Absorption Spectra

Figures 8-11 show examples of the spectra measured for each of the four photodeposited contaminants. The spectra are essentially featureless, although the three films from aromatic precursors (DC704, DEHP, and bisphenol) show a small shoulder between 250 and 300 nm. This shoulder is a clearly resolved peak in the spectrum of the DEHP precursor[10] and is assigned as a $\pi \rightarrow \pi^*$ transition (the "B band"), common to all aromatic compounds.[11]

Table 3 lists the total numbers of spectra, in each wavelength range, measured for each of the four films. Also shown is the maximum film thickness for each case.

Table 3. Accounting of spectra measured for the four photodeposited films.

Material	Wavelength Range	Number of Spectra	Maximum Thickness (nm)
Bisphenol	Visible	17	27
	Ultraviolet	15	
DC704	Visible	27	54
	Ultraviolet	24	
DEHP	Visible	15	46
	Ultraviolet	15	
Squalene	Visible	26	46
	Ultraviolet	21	

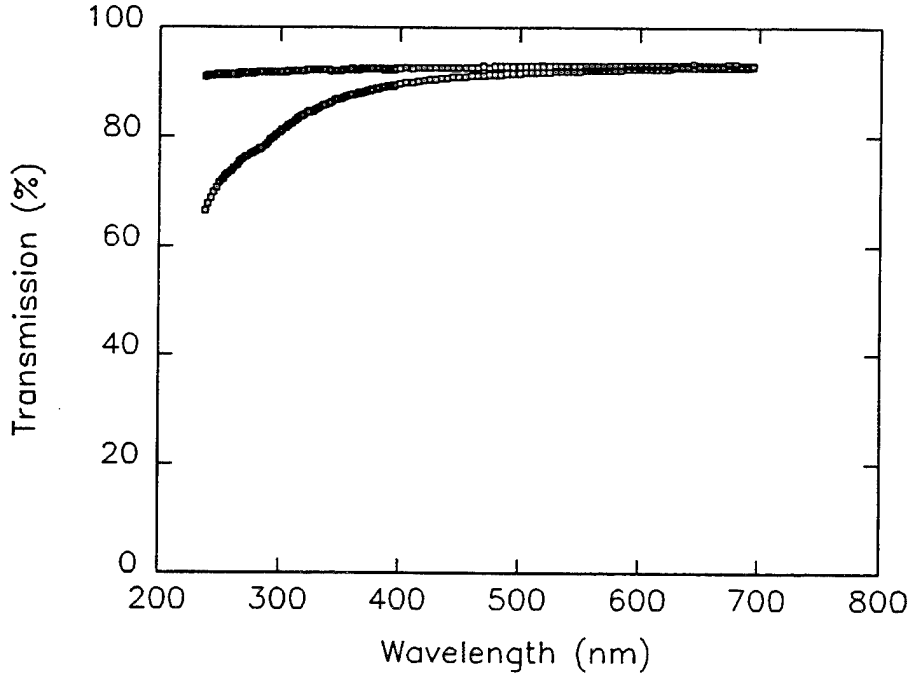

Figure 8. Typical transmission spectra measured during photodeposition of bisphenol. Top spectrum, clean 7940 substrate. Bottom spectrum ~22 nm of deposit.

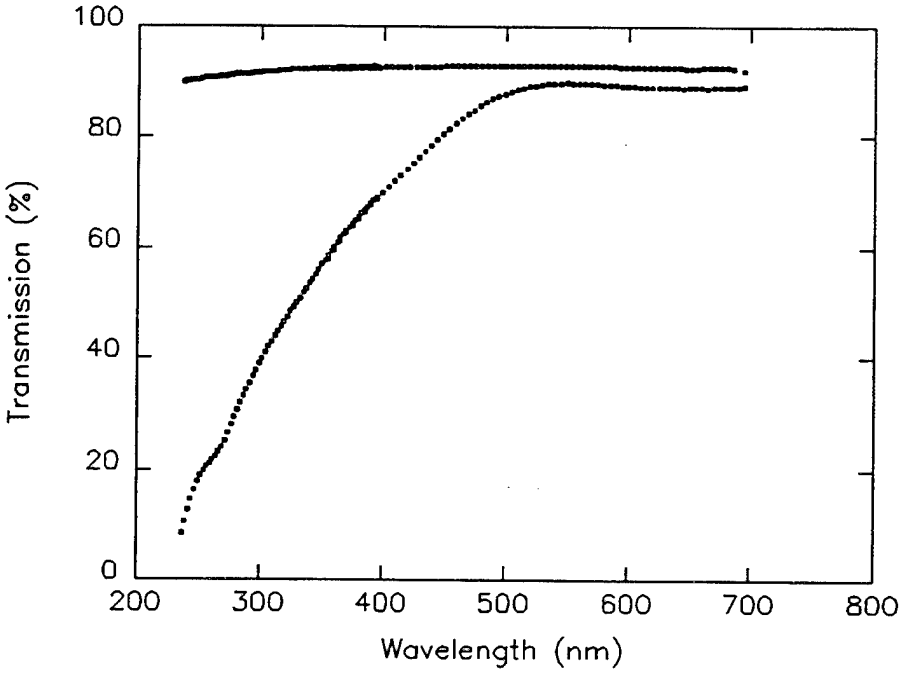

Figure 9. Typical transmission spectra measured during photodeposition of DC704. Top spectrum, clean 7940 substrate. Bottom spectrum ~55 nm of deposit.

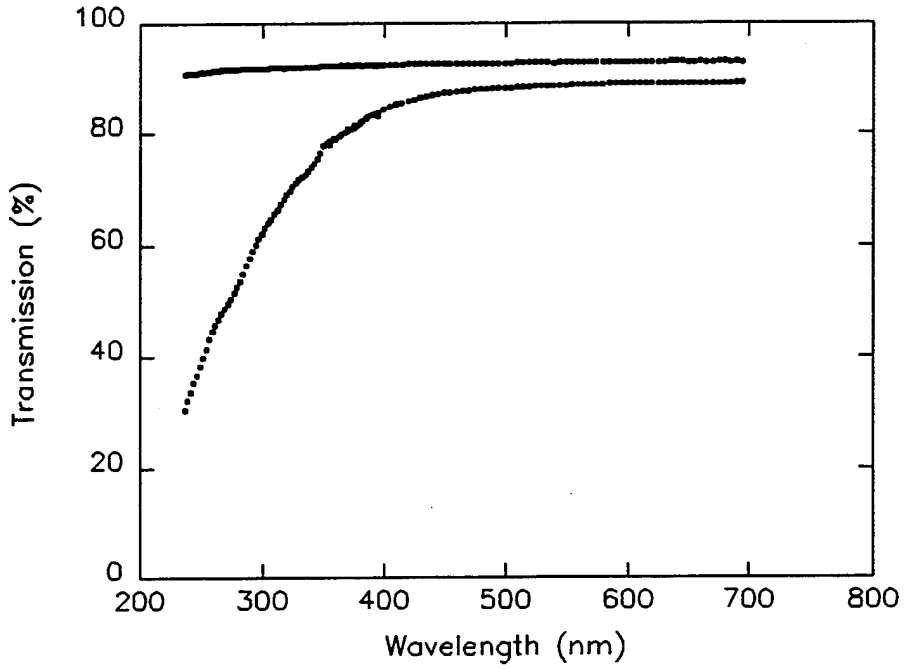

Figure 10. Typical transmission spectra measured during photodeposition of DEHP. Top spectrum, clean 7940 substrate. Bottom spectrum ~33 nm of deposit.

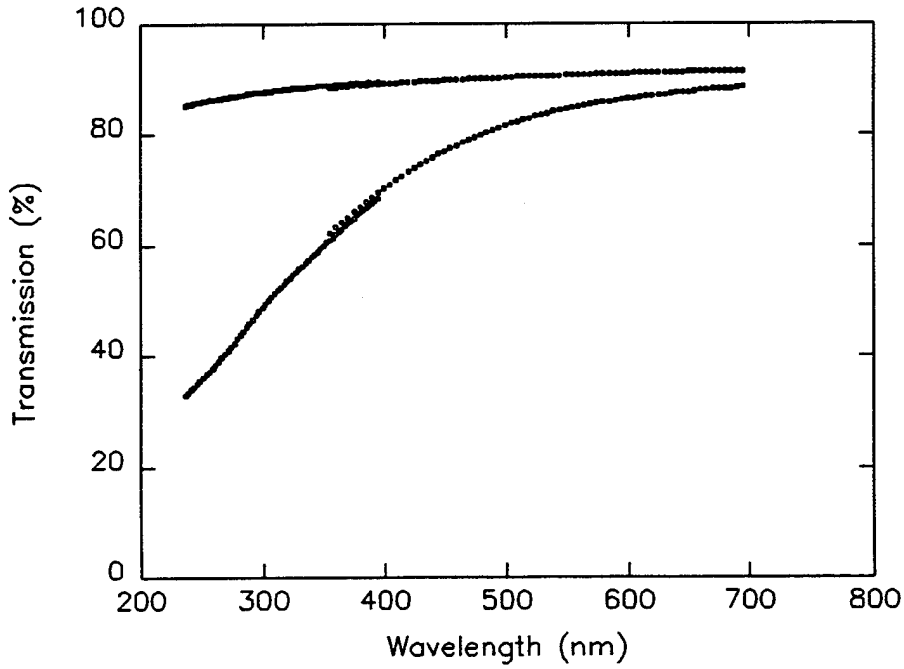

Figure 11. Typical transmission spectra measured during photodeposition of squalene. Top spectrum, clean 7940 substrate. Bottom spectrum ~46 nm of deposit.

3.2 Spectrum Fitting Approaches

Because the film spectra are essentially featureless*, the analysis of the data was carried out only every 5 nm in the visible range, and every 2.5 nm in the ultraviolet range.

In earlier data analyses, we attempted to fit the transmission vs thickness curves to the thin-film Fresnel equation and extract the wavelength-dependent complex index of refraction of the films.[6] However, as we acquired more data, we came to realize that the fits following this approach were not stable. There are two reasons for this. The first is the relatively small range of film thicknesses sampled: the range was not sufficient to observe interference fringes that would cause good convergence of the fit on the real part of the index of refraction. The second is that the films' optical properties appear to be changing during the course of the deposition. To test this hypothesis, we performed a second deposition of DEHP and followed it with a period of irradiation with the VUV lamps in the absence of a contaminant flux. We observed a continuous loss of film mass, accompanied by a continued increase in the optical density of the film.[12]

Therefore, we decided on a less complex approach to analyzing the spectra that assumes that all the observed transmission loss can be attributed to absorption of light by the film.** Note that, to the extent that this analysis describes the decline in transmission of a surface coated with the contaminant, the effect of the contaminant on a solar cell stack will be accurately described. The increase in solar absorptance of a thermal control coating will be estimated conservatively by this approach. Two approaches to this analysis are reported below.

3.2.1 Beer-Lambert Absorption Law Fits

The transmission spectra were fit to the Beer-Lambert absorption law,

$$\log_e(I/I_0) = -\alpha t \qquad (1)$$

where I/I_0 is the transmittance of the film, t is the film thickness, and α is the absorption coefficient of the film. The transmittance of the film was calculated as the ratio of the transmission of the deposit, on the substrate, to the transmission of the clean substrate. The quantity $\log(I/I_0)$ will be called the film absorbance.

---

* Other ways to describe these spectra include "boring," "brown," and "rather similar, one to another."

** Stated another way, we assumed that the film was "index matched" to the substrate.

Figures 12-15 present the examples of this analysis. The linear least-squares fits were not constrained to pass through the origin.* All of the fits are presented in the appendices along with numeric tabulations of the fitted absorption coefficients and intercepts of the plots.

Although there is a fair amount of scatter in the plots, the fits are remarkably satisfying. However, closer examination of the plots reveals that there is some curvature, and there is in some cases, a systematic failure of these fits to pass through the origin. These systematic departures from Beer's law result from a combination of noise inherent in the measurements and/or the probable continued darkening of the film during deposition.

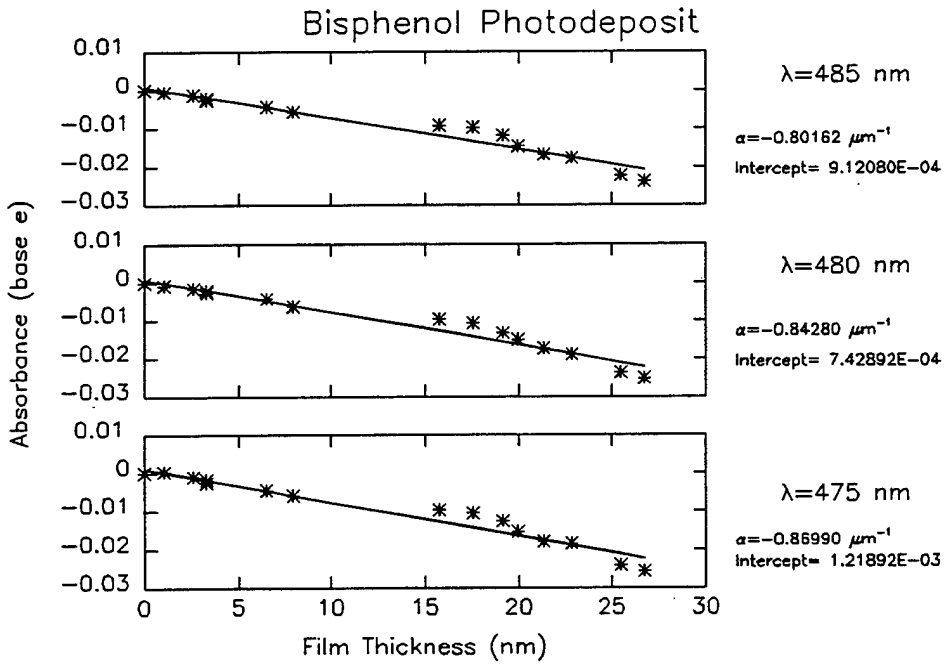

Figure 12. Example of a fit of bisphenol photodeposit transmission data to the Beer-Lambert absorption law. (See eq. 1)

* Note that, owing to a coding decision made early in the data analysis, the plots show the absorption coefficient as a negative number, which is opposite to the sign convention shown in equation 1.

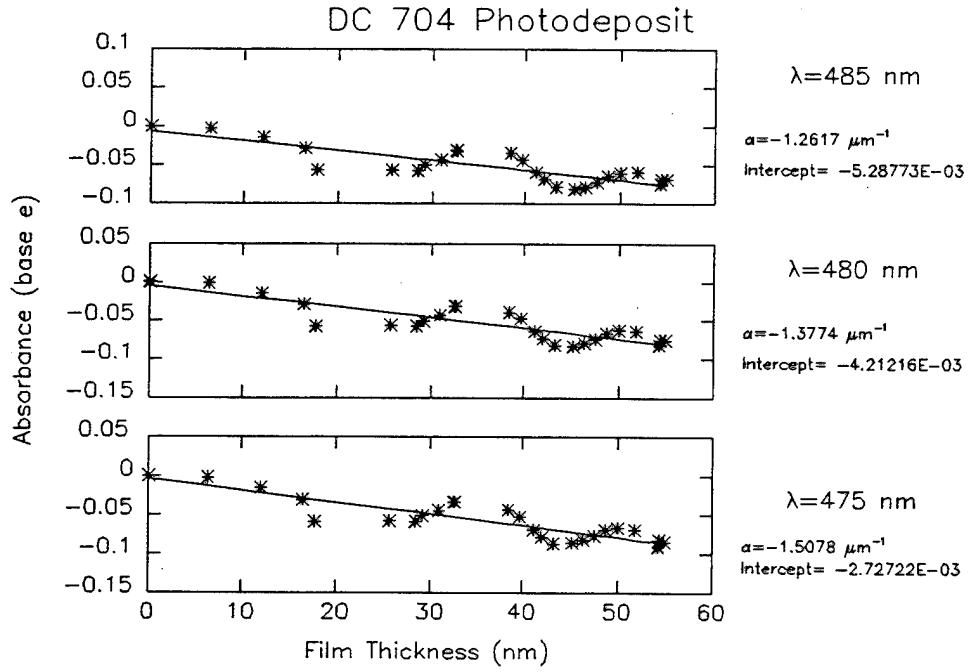

Figure 13. Example of a fit of DC704 photodeposit transmission data to the Beer-Lambert absorption law. (See eq. 1)

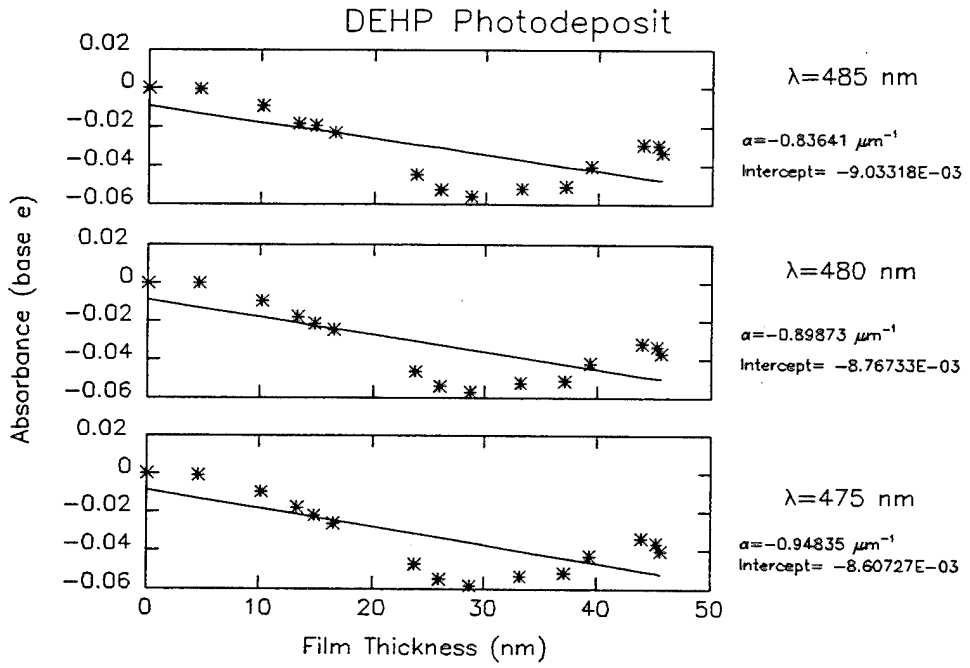

Figure 14. Example of a fit of DEHP photodeposit transmission data to the Beer-Lambert absorption law. (See eq. 1)

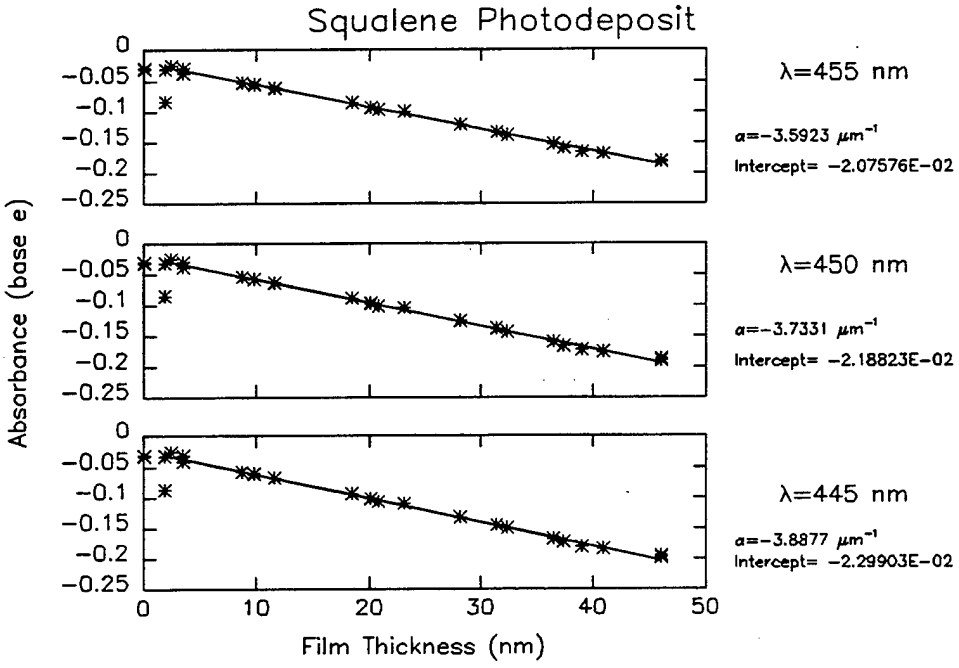

Figure 15. Example of a fit of squalene photodeposit transmission data to the Beer-Lambert absorption law. (See eq. 1)

3.2.2 Constrained Absorption Law Fits

Because data for some of the materials studied show curvature of the absorbance vs. thickness plots, a second approach was used to extract an apparent absorption coefficient from the data. In this case, the "Beer's law plot" is constrained to pass through the origin by calculating an apparent α as

$$\alpha = \langle \alpha_j \rangle = \frac{1}{j_f - j_i + 1} \sum_{j=j_i}^{j=j_f} \frac{\log_e [I(t_j)/I_0]}{t_j} \qquad (2)$$

where I/I_0 is the transmittance of the film, t_j is the film thickness for the j^{th} measurement, and α is the absorption coefficient of the film. The transmittance of the film was calculated as the ratio of the transmission of the deposit on the substrate to the transmission of the clean substrate.

Figures 16-19 show examples of this analysis approach. In calculating the averaged apparent absorption coefficient, $\langle \alpha_j \rangle$, data for thin films were omitted. All of the fits are presented in the appendices, along with numeric tabulations of the averaged absorption coefficients.

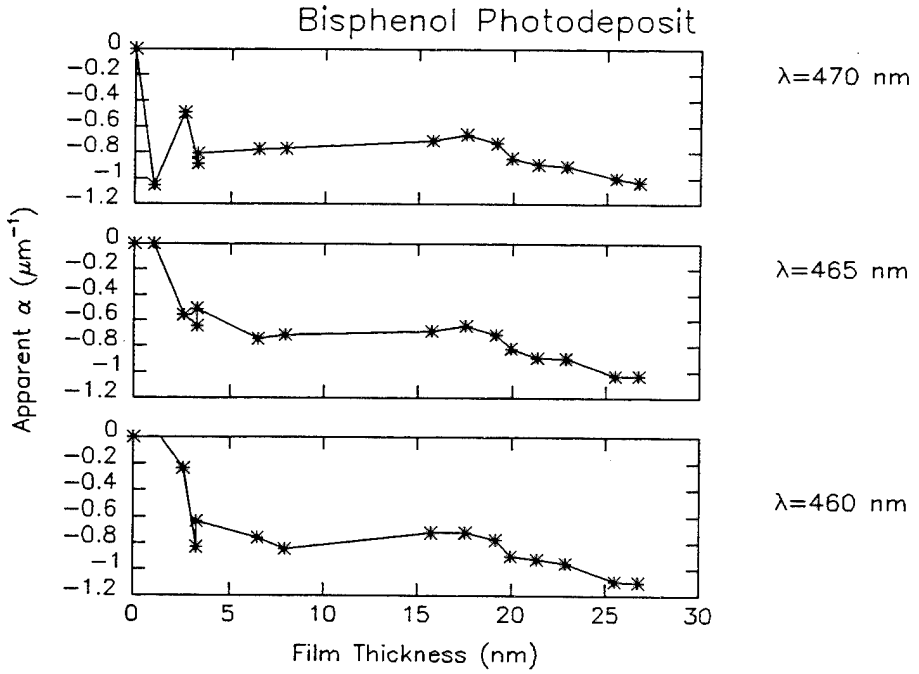

Figure 16. Example of a constrained fit of bisphenol photodeposit transmission data. (See eq. 2)

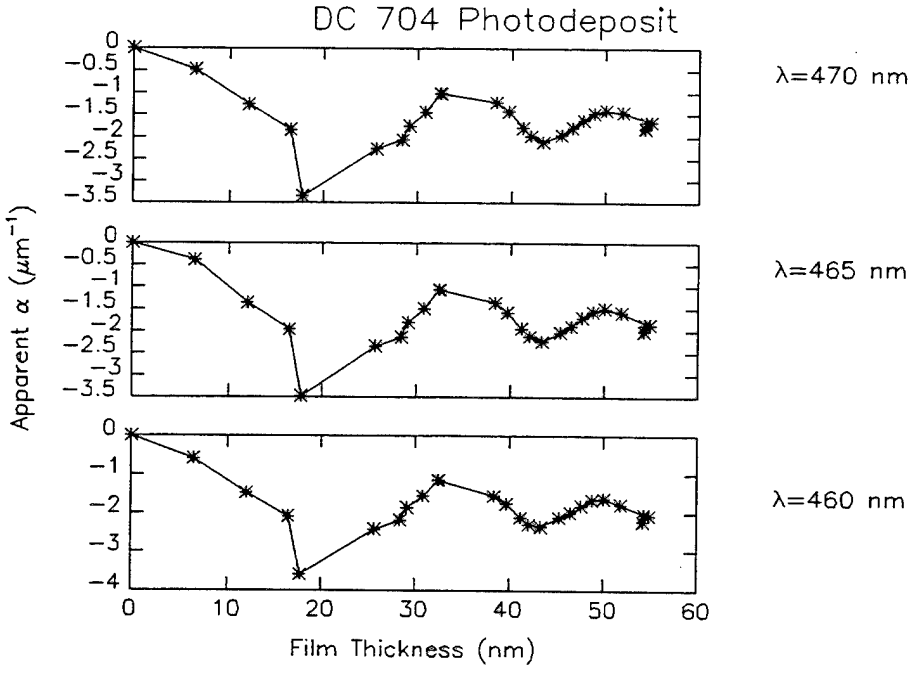

Figure 17. Example of a constrained fit of DC704 photodeposit transmission data. (See eq. 2)

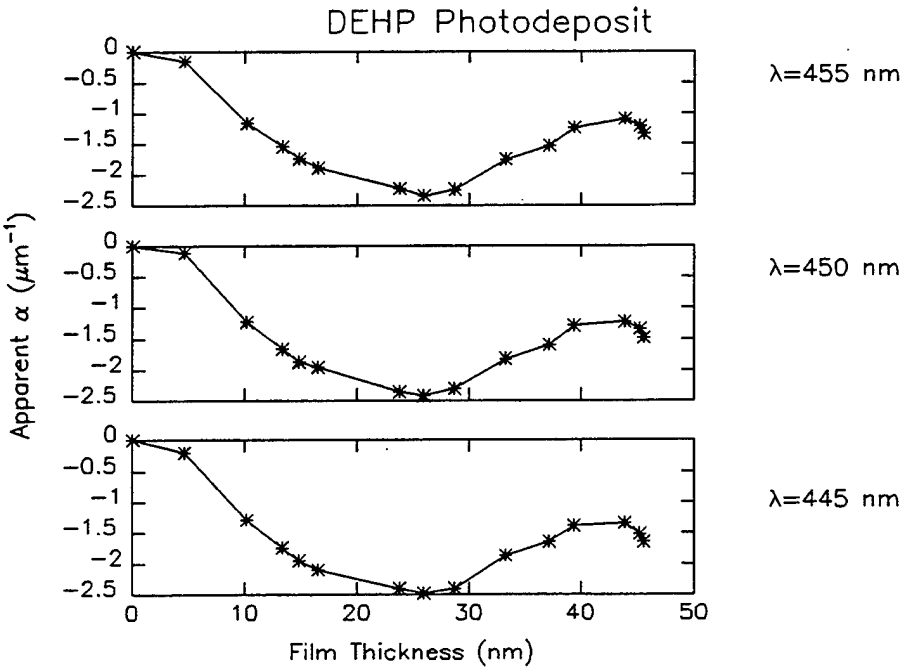

Figure 18. Example of a constrained fit of DEHP photodeposit transmission data. (See eq. 2)

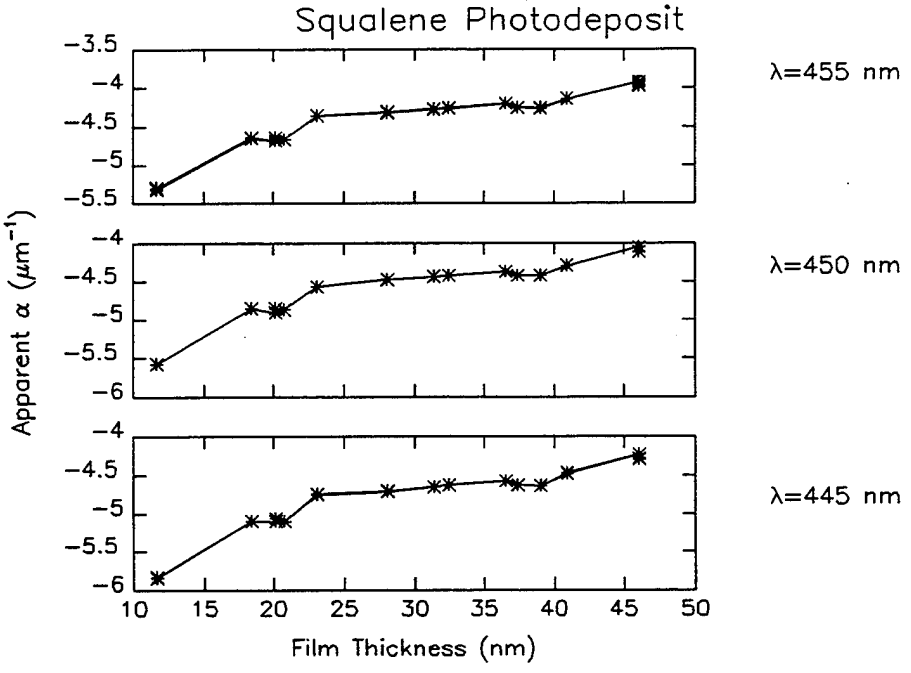

Figure 19. Example of a constrained fit of squalene photodeposit transmission data. (See eq. 2)

3.3 Spectrum Fitting Results

The results of the two fitting approaches are shown grapically in Figures 20-23. For all wavelengths and all materials, the extracted values of α agreed to within a factor of two.

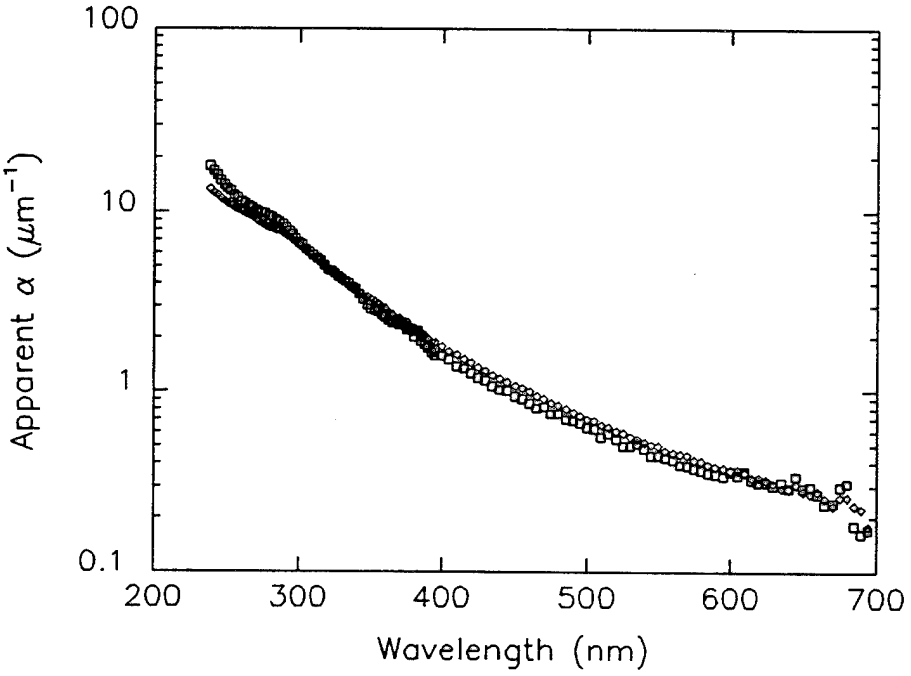

Figure 20. Comparison of Beer's law (diamonds) and constrained (squares) fits to the transmission spectra of the bisphenol photodeposit.

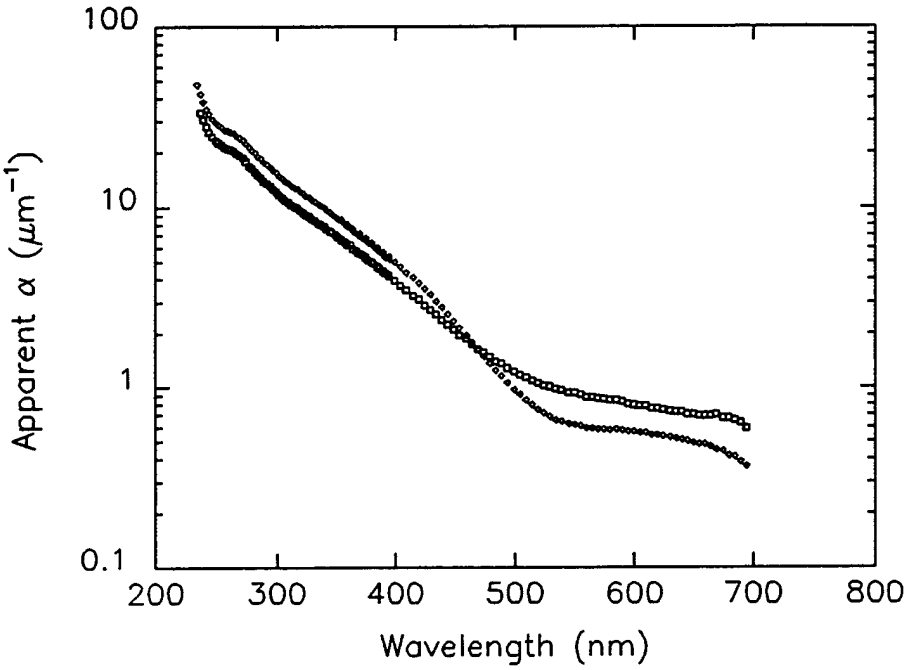

Figure 21. Comparison of Beer's law (diamonds) and constrained (squares) fits to the transmission spectra of the DC704 photodeposit.

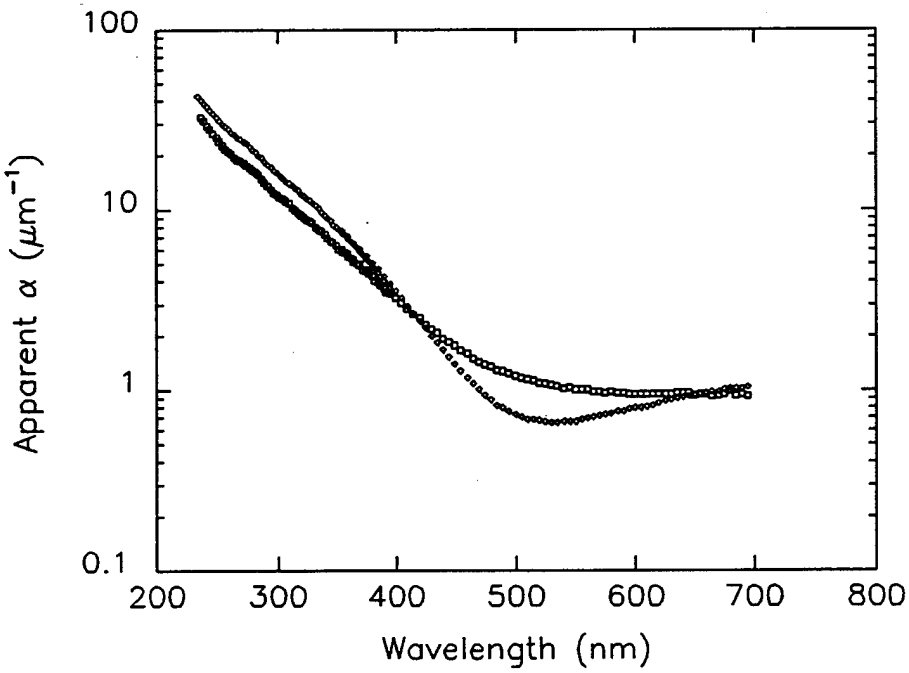

Figure 22. Comparison of Beer's law (diamonds) and constrained (squares) fits to the transmission spectra of the DEHP photodeposit.

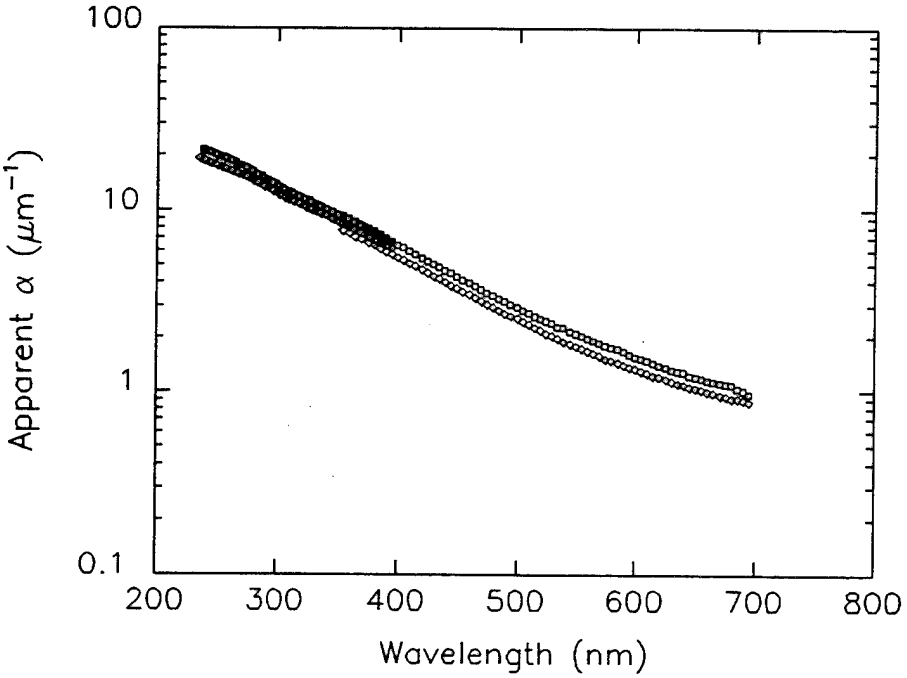

Figure 23. Comparison of Beer's law (diamonds) and constrained (squares) fits to the transmission spectra of the squalene photodeposit.

4. Discussion

4.1 Deposition Results

The greatest observed difference among the model contaminants studied thusfar is their propensity to photodeposit: some did and some did not. Once deposited, the films exhibit rather similiar transmission spectra.

The photochemical deposition results, described in Section 2 of this report, are summarized in Table 4. The columns labeled "molecular structure" describe the original assessment of the contaminant classes' propensity to interact with energetic particles in the space environment.[6] Note that the two classes expected to have medium-to-high interactions (phthalates and phenols) were observed to photodeposit. The aromatic hydrocarbons, expected to be good VUV absorbers, did not.

Earlier work in this laboratory showed that contaminant photodeposition under the conditions of these experiments can be described very well with a one-photon photochemistry model.[4] Therefore, the qualitative variation in photodeposition rate could have three origins: (1) the precursor molecule may be a poor absorber of the 150-180 nm radiation from the Xe resonance lamps; (2) the quantum yield for photodissociation or photoionization of the model contaminant may be low, even if the molecule is a strong absorber; or (3) the radical or ion fragment, if formed, may not be likely to undergo polymerization to form the tenaceous photodeposit. Future reports will address a literature-based study discerning the relative merits of these three explanations.

Table 4. Deposition Results: Comparison with *a priori* Contaminant Effects Prediction

Material	Model Contaminant	Molecular Structure*			Deposition
		Bond Strengths	Functional Groups	Ionization Trapping	
Phthalates	DEHP	M	M	H	YES
Phenols	bisphenol	H	H	H	YES
Polybenzimidizoles	n-phenylphthalimide	M	M	M	
Aromatic Hydrocarbons	bibenzyl	M	M	M	NO
	dodecahydrotriphenylene				NO
Aromatic Amines	tetradecylanaline	L	M	H	YES
Silicones	DC704	M	M	M	YES
Alkenes	squalene	H	L	L	YES
Aliphatic Carbonyls	10-nonadecanone	M	M	L	NO

* High (H), Medium (M), Low (L)

4.2 Contaminant Film Spectra

This report describes and archives fitting of the measured transmission spectra. More detailed analysis of the spectra and the contamination effects they imply for various spacecraft surfaces will be the subjects of future reports. However, to provide some context, the results of these measurements are briefly compared with the model contaminant spectrum used by a major U.S. spacecraft prime contractor's contamination analyst (Zeiner).[13]

Figures 24 and 25 show the comparison for the Beer's law and constrained analyses, respectively. Note that Zeiner's values for the imaginary part of the index of refraction, k, were converted to apparent absorption coefficients via the relationship[14]

$$\alpha = \frac{4\pi k}{\lambda} \tag{3}$$

where λ is the wavelength of light.

Zeiner's spectrum corresponds to an increase in solar absorptance of about 0.0035 per 10 nm of contaminant.[2] Clearly, the photodeposits measured here are more strongly absorbing. For example, Table 5 shows calculations of the apparent transmission of the Zeiner model and the bisphenol Beer's law fit for a single wavelength, 450 nm.* At this particular wavelength, the bisphenol film appears to absorb about 3 times as strongly as the Zeiner model. This sort of variation among contaminants in their effects has been observed, even on orbit.[2,15]

* Calculations for the Zeiner spectrum example were performed using the Multilayer Interference Program (MIP V1.3) by Sound Decisions, copyright 1986. The Zeiner model values were n=1.383, k=0.01934. A substrate index of 1.465, corresponding to fused silica, was assumed. The absorption coefficient of the bisphenol deposit is 1.1 μm^{-1}.

Table 5. Comparison of a Contractor Model and the Beer's Law Fit for Bisphenol at 450 nm.

Zeiner Spectrum @ 450 nm						Bisphenol (Beer's Fit)	
	Multilayer Interference Program Results			Apparent values*			
Thickness (nm)	Transmssion into substrate	Reflectance	Absorptance	Transmittance	Absorbance**	Absorbance	Transmittance
0	0.0356	0.9644	0	1	0	0	1
5	0.0359	0.9617	0.0025	0.9972	0.0028	0.006	0.9945
10	0.0358	0.9593	0.0049	0.9947	0.0053	0.011	0.9891
15	0.0355	0.9572	0.0073	0.9925	0.0075	0.017	0.9836
20	0.0348	0.9554	0.0098	0.9907	0.0094	0.022	0.9782
25	0.0338	0.9539	0.0123	0.9891	0.0109	0.028	0.9729
30	0.0326	0.9527	0.0148	0.9879	0.0122	0.033	0.9675
35	0.0311	0.9516	0.0173	0.9867	0.0134	0.039	0.9622
40	0.0295	0.9507	0.0198	0.9858	0.0143	0.044	0.9570
45	0.0278	0.9498	0.0224	0.9849	0.0153	0.050	0.9517
50	0.0260	0.9489	0.0250	0.9839	0.0162	0.055	0.9465

* Absorptance (a), reflectance (R), and transmittance (T) are related by $1 = a + R + T$.

** See equation 1.

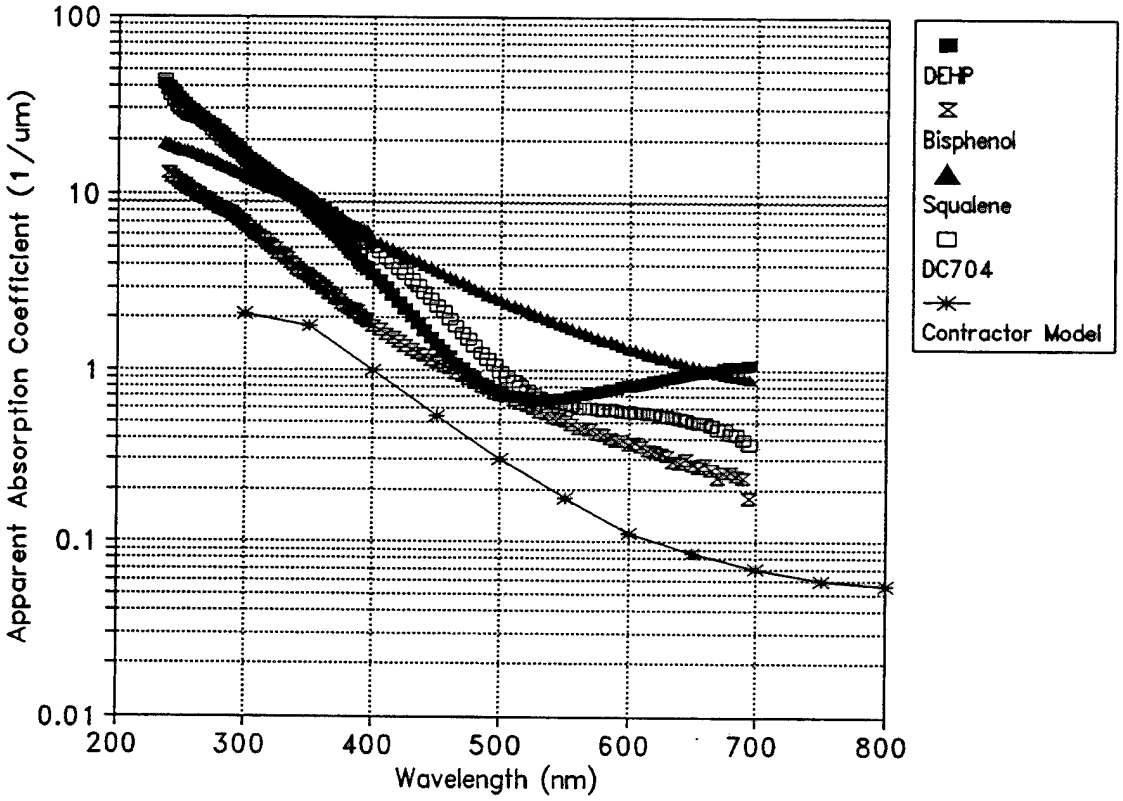

Figure 24. Comparison of apparent extinction coefficients of photodeposits of model contaminants obtained from Beer's law fits with the model spectrum used by a major space vehicle contractor.

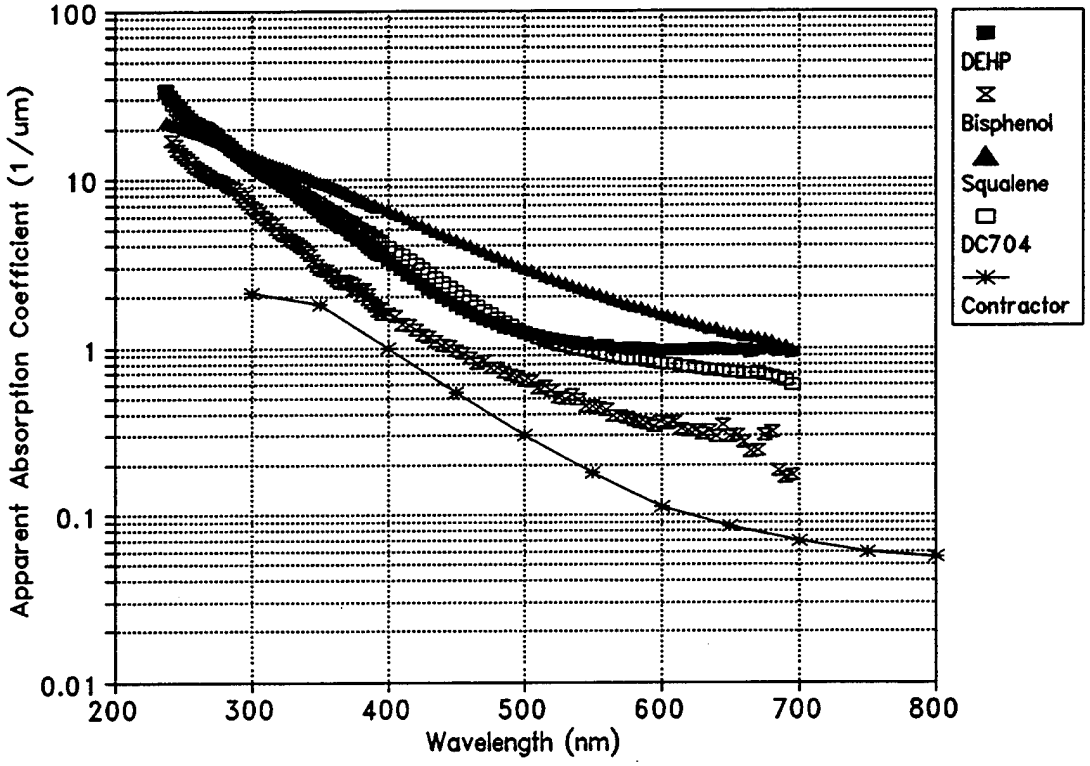

Figure 25. Comparison of apparent extinction coefficients of photodeposits of model contaminants obtained from the constrained fits with the model spectrum used by a major space vehicle contractor.

4.3 Future Work

This report archives the photochemical deposition and optical transmission spectra for several classes of model spacecraft contaminants. Throughout the body of this report, several areas of ongoing and future research and analysis have been indicated. The most significant are recapitulated here.

a. *Photodeposition Rates*: The greatest variation among the types of contaminants studied was whether they photodeposited under 150-180 nm irradiation. A literature review of VUV absorption cross-section data and quantum yields is required to illucidate this important observation.

b. *Optical Spectra*: The similarity of the optical transmission spectra recorded indicates that the photodeposits may be tending toward similar ultimate compositions under VUV irradiation. A literature-based comparison of the measured spectra to the spectra of amorphous and graphitic carbon will be performed to help explain these data. In addition, a literature review of similar laboratory data from other studies of contaminant film effects is needed to complete this work.

c. *Optical Effects*: Integration of the measured spectra over the solar spectrum is needed to calculate the effects of the various photodeposits on specific spacecraft surfaces. These included silverized fused silica optical solar reflectors, silverized ceria-doped microsheet optical solar reflectors, silicon and gallium arsenide solar photovoltaic stacks, and white spacecraft thermal control paints.

In addition to these analytical efforts, laboratory measurements of additional classes of contaminants are in progress.

References

1. T.B. Stewart, G.S. Arnold, D.F. Hall, D.C. Marvin, W.C. Hwang, and R.D. Chandler, "Photochemical Spacecraft Self Contamination: Laboratory Results and Systems Impacts," *J. Spacecraft*, 26, 358-366, (1989).

2. D.F. Hall, "Current Flight Results from the P78-2 (SCATHA) Spacecraft Contamination and Coatings Degradation Experiment," *Proceedings of an International Symposium on Spacecraft Materials in Space Environment*, ESTEC, Noordwijk, Holland, 1982., pp 143-148.

3. J.M. Dowling, M.M. Hills, G.S. Arnold, and H.K.A. Kan, "Contamination Effects on Surveillance Telescopes," SMC-TR-94-01, The Aerospace Corporation, TR-93(3935)-14, El Segundo, CA, 22 October 1993.

4. T.B. Stewart, G.S. Arnold, D.F. Hall, and H.D. Marten, "Absolute Rates of Vacuum Ultraviolet Photochemical Deposition of Organic Films," *J. Phys. Chem.*, **93**, 2392, (1989).

5. Anon, "Standard Test Method for Contamination Outgassing Characteristics of Spacecraft Materials," ASTM E 1559-93, American Society for Testing of Materials, Philadelphia, PA, 15 August 1993. (This test method is under the jurisdiction of the ASTM Committee E-21 on Space Simulation and Application of Space Technology, and is the direct responsibility of Subcommittee E21.05 on contamination.)

6. H.S. Judeikis, G.S. Arnold, M. Hill, R.C. Young Owl, and D.F. Hall, "Design of a Laboratory Study of Contaminant Film Darkening in Space," *Scatter from Optical Components- Proceedings of the Society of Photo-Optical Instrumentation Engineers*, 1165, 406-423, San Diego, CA, 8-10 August 1989.

7. G.S. Arnold, R.C. Young Owl, and D.F. Hall, "Optical Effects of Photochemically Deposited Contaminant Films," *Optical System Contamination: Effects, Measurement, and Control- Proceedings of the Society of Photo-Optical Instrumentation Engineers*, 1329, 255-265, San Diego, CA, 10-12 July 1990.

8. A.P.M. Glassford, "Practical Model for Molecular Contaminant Deposition Kinetics," J. Thermophysics and Heat Transfer, Vol. 6, No. 4, pp. 656-664, Oct.-Dec. 1992

9. A. P. M. Glassford, "Application of the quartz crystal microbalance to space system contamination studies," Chapt. 9 of Applications of Piezoelectric Quartz Crystal Microbalances, C. Lu and A. W. Czanderna, Eds., Elsevier, New York, 1984.

10. J.A. Colony, "Ultraviolet Absorption of Common Spacecraft Contaminants," NASA TM 80551, NASA Goddard Space Flight Center, Greenbelt, MD, (1979).

11. D.J. Pasto and C.R. Johnson, *Organic Structure Determination*, Prentice Hall, Englewood Cliffs, NJ, pp. 99-101, (1969).

12. K. Luey and G.S. Arnold, to be published.

13. E.N. Zeiner, Hughes Aircraft Co., private communication. The data used by Dr. Zeiner were originally collected by Dr. Robert Champetier of The Aerospace Corporation, who reported apparent absorption coefficients. Zeiner then developed values for the real part of the index via Kramers-Kronig analysis.

14. G. Hass, "Optical Properties of Metals," in *The American Institute of Physics Handbook*, D.E. Gray, Ed., McGraw-Hill, New York, p **6**-118, (1972).

15. C.C. anderson and M.M. Hattar, "Calorimetric Measurements of Thermal Control Surface at Geosynchronous Orbit," *J. Thermophysics*, 2, 145-151, (1988).

TECHNOLOGY OPERATIONS

The Aerospace Corporation functions as an "architect-engineer" for national security programs, specializing in advanced military space systems. The Corporation's Technology Operations supports the effective and timely development and operation of national security systems through scientific research and the application of advanced technology. Vital to the success of the Corporation is the technical staff's wide-ranging expertise and its ability to stay abreast of new technological developments and program support issues associated with rapidly evolving space systems. Contributing capabilities are provided by these individual Technology Centers:

Electronics Technology Center: Microelectronics, VLSI reliability, failure analysis, solid-state device physics, compound semiconductors, radiation effects, infrared and CCD detector devices, Micro-Electro-Mechanical Systems (MEMS), and data storage and display technologies; lasers and electro-optics, solid state laser design, micro-optics, optical communications, and fiber optic sensors; atomic frequency standards, applied laser spectroscopy, laser chemistry, atmospheric propagation and beam control, LIDAR/LADAR remote sensing; solar cell and array testing and evaluation, battery electrochemistry, battery testing and evaluation.

Mechanics and Materials Technology Center: Evaluation and characterization of new materials: metals, alloys, ceramics, polymers and composites; development and analysis of advanced materials processing and deposition techniques; nondestructive evaluation, component failure analysis and reliability; fracture mechanics and stress corrosion; analysis and evaluation of materials at cryogenic and elevated temperatures; launch vehicle fluid mechanics, heat transfer and flight dynamics; aerothermodynamics; chemical and electric propulsion; environmental chemistry; combustion processes; spacecraft structural mechanics, space environment effects on materials, hardening and vulnerability assessment; contamination, thermal and structural control; lubrication and surface phenomena; microengineering technology and microinstrument development.

Space and Environment Technology Center: Magnetospheric, auroral and cosmic ray physics, wave-particle interactions, magnetospheric plasma waves; atmospheric and ionospheric physics, density and composition of the upper atmosphere, remote sensing using atmospheric radiation; solar physics, infrared astronomy, infrared signature analysis; effects of solar activity, magnetic storms and nuclear explosions on the earth's atmosphere, ionosphere and magnetosphere; effects of electromagnetic and particulate radiations on space systems; space instrumentation; propellant chemistry, chemical dynamics, environmental chemistry, trace detection; atmospheric chemical reactions, atmospheric optics, light scattering, state-specific chemical reactions and radiative signatures of missile plumes, and sensor out-of-field-of-view rejection.